ELSEVIER

Earth and Planetary Science Letters 207 (2003) 165–179

EPSL

www.elsevier.com/locate/epsl

Rheological behavior of bubble-bearing magmas

Rajinder Pal

Department of Chemical Engineering, University of Waterloo, Waterloo, ON, Canada N2L 3G1

Received 15 August 2002; received in revised form 16 October 2002; accepted 14 November 2002

Abstract

The vesiculation of the rising magma in a volcanic conduit results in a large change in the viscosity of magma. Understanding the effect of bubbles on the viscous behavior of bubble–melt mixtures over a wide range of bubble volume fractions is essential for accurate modeling of the volcanic processes. In this study, new equations for the relative viscosity of concentrated bubble-bearing suspensions are developed using a differential scheme along with the solution of an infinitely dilute suspension of bubbles. Out of the four models developed in the paper, two models predict the relative viscosity to be a function of only two variables: capillary number and volume fraction of bubbles. There are no adjustable parameters in these models. The remaining two models include an additional parameter, that is, the maximum packing volume fraction of bubbles. The proposed models are evaluated using published numerical and experimental data on the relative viscosity of concentrated suspensions of bubbles. The viscosity models for bubble-bearing suspensions developed in this study are useful in modeling of the volcanic processes.

Keywords: rheology; bubble-bearing magmas; capillary number; suspensions; viscosity; emulsions

1. Introduction

Knowledge of the rheological properties of magmas is required for accurate modeling of the volcanic processes [1–15]. For instance, rheological data are needed to quantify volatile exsolution, bubble growth rates and explosivity of volcanic eruptions [12]. During an eruption, as the magma rises through a volcanic conduit towards the Earth's surface, nucleation and growth of gas bubbles occur by exsolution of volatiles (mainly water and carbon dioxide) that were initially dissolved in magma at high pressures [16–31]. Several experimental studies have been conducted on bubble growth in natural melts [16–23]. In addition to experimental studies, many bubble growth models have been developed [24–29]. Bubble nucleation in volcanic eruptions occurs due to supersaturation of volatiles during magma ascent. Nucleation of bubbles is greatly enhanced by the presence of heterogeneities (such as crystals) in the melt [19]. The level of supersaturation required to allow bubble nucleation depends on the presence and abundance of such heterogeneities. Once bubbles are formed, their growth in magma is controlled by decompression and diffusion processes. Decompressional growth of bubbles occurs because of changes in hydrostatic pressure as the magma rises towards the surface. Diffusional growth is due to diffusion of the volatiles from the melt to the bubbles through the

E-mail address: rpal@engmail.uwaterloo.ca (R. Pal).

0012-821X/02/$ – see front matter © 2002 Published by Elsevier Science B.V.
doi:10.1016/S0012-821X(02)01104-4

melt–vapor interface. Diffusional growth rates are governed by factors such as viscosity of melt, solubilities of volatiles in the melt, concentration of dissolved volatiles, and the degree of supersaturation of volatiles [28].

Fig. 1 summarizes the main processes occurring in a volcanic conduit [7]. In the initial portion of the conduit, there occurs single-phase flow. After the initial single-phase flow region comes the two-phase 'bubbly flow' region where bubbles nucleate and grow. At the end of the bubbly section, the magmatic emulsion fragments and turns into a gas consisting of small particles (ash), which may be liquid or partially solid. The size of these particles varies inversely with the intensity of the eruption.

Our current understanding of the 'bubbly' region is somewhat limited [7]. In this region, the vesiculation of the rising magma drastically changes the physico-chemical properties and rheology of magma within the conduit, and therefore the ascent rate of magma. The viscosity of bubbly magma (η) is the product of melt viscosity (η_c) and the relative viscosity of bubble–melt mixture (η_r), that is, $\eta = \eta_c \eta_r$. The relative viscosity of bubbly magma depends on the volume fraction of bubbles in the magma as well as on the capillary number. The viscosity of the melt, on the other hand, is dependent on the volatile content. In actively vesiculating flows, as is the situation in volcanic conduit, the changes in the magma viscosity (η) are dominated by massive changes in the melt viscosity (η_c); the melt viscosity is known to increase by several orders of magnitude [8] during the ascent of magma due to exsolution of volatiles. However, in surface propagation of lava flows, viscosity of the bubbly magma is strongly influenced by bubble content and capillary number.

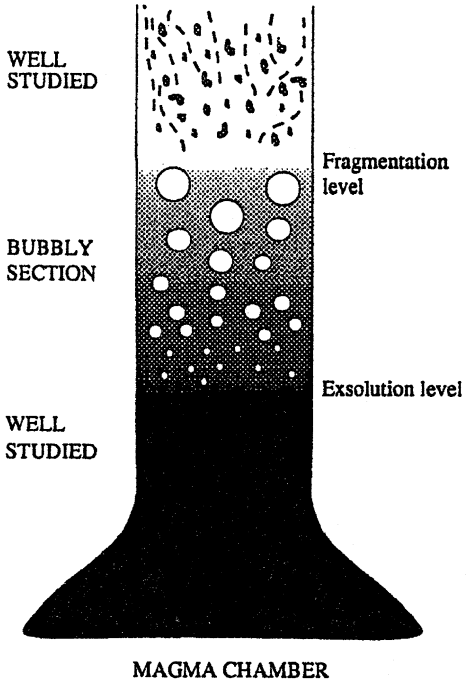

Fig. 1. Schematic representation of the different parts of the volcanic conduit [7].

The viscous behavior of pure melts (without bubbles) is comparatively well known; the melt viscosity is known to be a function of its chemical composition, volatile and crystal contents, temperature and pressure [11]. By contrast, the effects of bubbles on the viscous properties of magmas are not well understood. Understanding the effect of bubbles on the viscosity behavior of bubble–melt mixtures over a wide range of bubble volume fractions is essential to better constrain the behavior of magma during decompression, ascent, eruption, and emplacement on Earth and other planetary bodies [15].

2. Brief background

The viscosity of suspensions of two immiscible fluids generally depends on the following factors: (a) particle Reynolds number (N_{Re}), defined as the ratio of inertial force to viscous force [32]; (b) ratio of dispersed-phase viscosity to continuous-phase viscosity, λ [33–36]; (c) capillary number (N_{Ca}), defined as the ratio of shear stress to interfacial stress [5,6,10,11,37]; (d) volume fraction of dispersed particles, ϕ [5,6,10,11,33–37]; (e) rheology of continuous-phase fluid [38]; (f) particle size distribution [39]; and (g) concentration of surfactant, if present [40]. In bubbly magmatic flows, some of these factors are not impor-

tant. For instance, the viscosity ratio λ is essentially zero; the bubble Reynolds number is virtually always $\ll 1$ [15]; the continuous-phase fluid is generally Newtonian over a wide range of stresses and strain rates [37], and there are no surfactants present in the system. Thus, the viscosity of bubble-bearing magmas is expected to be a function of the following three variables: capillary number, volume fraction of bubbles, and bubble size distribution.

The capillary number (N_{Ca}) in natural magmatic flows spans a broad range of 10^{-2}–10^{3} due to large variations in melt viscosity and shear rates [10,15]. Bubble volume fraction (ϕ) can range from 0 to $\sim$0.9 [37]. The increase in ϕ can increase or decrease the viscosity of bubble–melt mixture depending upon the capillary number. Furthermore, in bubbly magmatic flows, bubbles are rarely of uniform size. Studies of natural pumice clasts show a broad range of bubble sizes [20,26–37,39]. The bubble size distribution can have a significant effect on the viscosity of bubble–melt mixtures, especially at high volume fractions of bubbles [11,26,39].

Despite the importance of the problem, there are no commonly accepted theoretical or empirical models available in the literature to describe the viscous behavior of concentrated bubbly suspensions. In a recent publication, Llewellin et al. [37] have proposed a semi-empirical constitutive equation for bubbly suspensions with gas volume fractions $\phi < 0.5$. In the limit of $N_{Ca} \rightarrow 0$, their equation gives:

$$\tau_{ij} = \eta_c(1 + 9\phi)\dot{\gamma}_{ij} \quad (1)$$

where τ_{ij} is the deviatoric stress tensor, η_c is the continuous-phase viscosity, and $\dot{\gamma}_{ij}$ is the strain rate tensor. The term (1+9ϕ) in Eq. 1 was arrived at on the basis of oscillatory shear data obtained experimentally on bubbly suspensions in a parallel plate geometry. One problem with Llewellin et al.'s equation (Eq. 1) is that it fails to obey the well-known Taylor's Law [41] for dilute emulsions. According to Taylor's Law, the viscosity of a dilute bubbly suspension (η) is given by:

$$\eta = \eta_c(1 + \phi) \quad (2)$$

Several factors could be responsible for the high values of viscosity obtained by Llewellin et al.; one of them is the 'creaming/bubble-rise effect' in bubbly suspensions. Pal [42] found that the rheological properties of oil-in-water emulsions can be strongly influenced by creaming of oil droplets in viscometers such as the parallel plate type used by Llewellin et al. Further discussion on anomalous behavior of Llewellin et al.'s [37] bubbly suspensions is given in Section 4 of this paper.

Clearly, there is a need to develop models for the viscosity of concentrated bubbly suspensions. In this article, **new** viscosity models for concentrated bubbly suspensions are developed. The models developed are consistent with the exact theories of Taylor [41] and Frankel and Acrivos [43] for dilute systems. Although the models developed are independent of any experimental measurements, they are quite capable of describing the available numerical and experimental data on bubbly suspensions.

3. New viscosity equations for concentrated bubbly suspensions

New viscosity equations for concentrated bubbly suspensions are derived using the differential scheme originally proposed by Brinkman [44] and Roscoe [45] to derive the viscosity equations for concentrated suspensions of *rigid* spherical particles. According to this approach, a concentrated suspension is considered to be obtained from an initial continuous phase by successively adding infinitesimally small quantities of particles to the system while the final volume fraction of the dispersed phase is reached. At any arbitrary stage (i) of the process, the addition of an infinitesimal amount of particles leads to the next stage (i+1). The suspension of stage (i) is then treated as an equivalent 'effective medium' which is homogeneous with respect to the new set of particles added to reach stage (i+1). The solution of a dilute suspension system is applied to determine the incremental increase in viscosity in going from stage (i) to stage (i+1). Brinkman [44] and Roscoe [45] utilized the celebrated Einstein equation [46,47] for the viscosity of dilute suspension of rigid spherical particles, as a solution for the dilute

suspension system. The differential equation derived in this manner is integrated to obtain the final solution. In the present work, the Brinkman–Roscoe differential scheme is applied to the Frankel and Acrivos equation (discussed below) in order to derive the viscosity equations for concentrated suspensions of deformable bubbles.

3.1. Frankel and Acrivos's exact theory for dilute bubbly suspensions

Frankel and Acrivos [43] derived an exact rheological constitutive equation for a dilute emulsion of uniform (same size) droplets of a Newtonian fluid in another such fluid of different viscosity. As creeping flow equations were used in the derivation, the constitutive equation of Frankel and Acrivos is valid for particle Reynolds number (N_{Re}) $\ll 1$. For bubbly suspensions (magmatic emulsions), where the ratio of dispersed-phase viscosity to continuous-phase viscosity is essentially zero, the Frankel and Acrivos equation (equation 3.12 on p. 73 of their paper) becomes:

$$\overline{\tau} + \Lambda\frac{D\overline{\tau}}{Dt} = 2\eta_c(1+\phi)\left(\overline{d} + \Lambda\frac{D\overline{d}}{Dt}\right) + \left(\frac{\eta_c^2 R}{\sigma}\right) \phi\left\{\left(\frac{-32}{5}\right)\frac{D\overline{d}}{Dt} + \left(\frac{24}{35}\right)\left[(\overline{d}\cdot\overline{d}) + (\overline{d}^{T}\cdot\overline{d}^{T}) - \frac{2}{3}\mathrm{tr}(\overline{d}\cdot\overline{d})\overline{\delta}\right]\right\} \quad (3)$$

where $\overline{\tau}$ is the deviatoric stress tensor, $\overline{d}$ is rate of deformation tensor, $\overline{\delta}$ is unit tensor, $\overline{d}^{T}$ is transpose of $\overline{d}$, tr refers to trace of a tensor, η_c is continuous-phase (matrix) viscosity, R is bubble radius, σ is interfacial tension between the two phases, ϕ is volume fraction of bubbles, Λ is equal to $(6\eta_c R/5\sigma)$, and D/Dt is the Jaumann derivative. Eq. 3 is applicable for steady or for weakly time-dependent flows.

The viscosity of materials, by definition, is the ratio of shear stress to shear rate when the material is subjected to steady viscometric flow (simple shear flow). When a bubbly suspension is subjected to steady viscometric flow, Eq. 3 gives the following expression for the viscosity of bubbly magmas (see Appendix A):

$$\eta_r = \frac{\eta}{\eta_c} = 1 + \phi\left[\frac{1-\left(\frac{12}{5}\right)N_{Ca}^2}{1+\left(\frac{6}{5}N_{Ca}\right)^2}\right] \quad (4)$$

where η_r is the relative viscosity, defined as the ratio of suspension viscosity (η) to matrix viscosity (η_c), and N_{Ca} is the capillary number, defined as:

$$N_{Ca} = \frac{R\eta_c\dot{\gamma}}{\sigma} \quad (5)$$

In Eq. 5, $\dot{\gamma}$ is the shear rate. Strictly speaking, the Frankel and Acrivos equations (Eqs. 3 and 4) are applicable for small deformations. Because of the mathematical complexities involved, the theoretical studies published on emulsion rheology generally assume small deformation of droplets. Nevertheless, Eq. 4 can be applied to high capillary numbers as an approximation provided that the bubbles do not rupture. The experimental data of Rust and Manga [10] on steady shear viscosity of dilute bubbly suspensions clearly demonstrates the applicability of Eq. 4 to high capillary numbers as an approximation. As the ratio of dispersed-phase viscosity to continuous-phase viscosity for bubble-bearing magmas is very small, bubbles with such low viscosity ratios are expected to reach a stable shape rather than rupture in steady shear flow up to capillary number as high as 10^3 [23].

In the limit $N_{Ca} \to \infty$, the Frankel and Acrivos equation (Eq. 4) gives:

$$\eta_r = 1 - \frac{5}{3}\phi \quad (6)$$

Eq. 6 indicates that at high capillary numbers, η_r decreases with the increase in ϕ. This trend is observed in several numerical and experimental studies published in the literature [1,6,10,15]. It should also be noted that Eq. 6 can be derived directly from the shear modulus equation for dilute bubbly suspension, using the analogy between shear viscosity and shear modulus [37,48–49]. In the limit of $N_{Ca} \to 0$, Eq. 4 gives the well-known Taylor's Law [41], that is, Eq. 2. According to Taylor's Law, the viscosity of a suspension increases with the increase in ϕ.

3.2. New viscosity equations for concentrated bubbly suspensions

The Frankel and Acrivos viscosity equation (Eq. 4) cannot be applied at finite concentrations of dispersed phase (bubbles) as the hydrodynamic interaction between the bubbles is ignored in its derivation. Eq. 4 is probably valid for ϕ less than about 0.05 (especially in the limit of $N_{Ca} \rightarrow 0$). In order to derive the viscosity equations for concentrated suspensions of bubbles, the Brinkman–Roscoe differential scheme is applied to the Frankel and Acrivos equation (Eq. 4).

Let us now consider a suspension of bubbles with a volume fraction of bubbles ϕ. Into this suspension, an infinitesimally small amount of new bubbles is added. The increment change in viscosity $d\eta$ resulting from the addition of the new bubbles can be calculated from the solution of a dilute system, that is, Eq. 4, by treating the suspension into which new bubbles are added as an equivalent effective medium of viscosity η. Thus:

$$d\eta = \eta \left[\frac{1-\frac{12}{5}\left(\frac{\dot{\gamma}\eta R}{\sigma}\right)^2}{1+\left(\frac{6}{5}\frac{\dot{\gamma}\eta R}{\sigma}\right)^2} \right] d\phi \quad (7)$$

This equation can be rewritten as:

$$\frac{d\eta}{\eta\left[1-\frac{12}{5}\left(\frac{\dot{\gamma}\eta R}{\sigma}\right)^2\right]} + \frac{\left[\left(\frac{6}{5}\frac{\dot{\gamma}\eta R}{\sigma}\right)^2\right]}{\eta\left[1-\frac{12}{5}\left(\frac{\dot{\gamma}\eta R}{\sigma}\right)^2\right]} d\eta = d\phi \quad (8)$$

Upon integration with the limit $\eta \rightarrow \eta_c$ at $\phi \rightarrow 0$, Eq. 8 gives:

$$\eta_r \left[\frac{1-\frac{12}{5}\eta_r^2 N_{Ca}^2}{1-\frac{12}{5}N_{Ca}^2} \right]^{-4/5} = \exp(\phi) \quad (9)$$

Eq. 9, referred to as 'model 1' in the remainder of the paper, reduces to the following equations:

$$N_{Ca} \rightarrow 0, \quad \eta_r = \exp(\phi) = 1 + \phi + \frac{\phi^2}{2} + \ldots \quad (10)$$

$$N_{Ca} \rightarrow \infty, \quad \eta_r = \exp\left(\frac{-5}{3}\phi\right) = 1 - \frac{5}{3}\phi + \frac{25}{18}\phi^2 + \ldots \quad (11)$$

Thus, model 1 is consistent with the results for a dilute system.

Model 1 is expected to describe the viscosity of bubbly suspensions at low to moderate values of ϕ ($\phi \leq 0.20$). At high ϕ, model 1 is expected to underpredict η_r at low N_{Ca} and overpredict η_r at high N_{Ca}. This is because in the derivation of the differential equation (Eq. 7) leading to model 1 (Eq. 9), it is assumed that the whole volume of the suspension before new bubbles are added is available as free volume to the new bubbles. In reality, the free volume available to disperse the new bubbles is significantly less, due to the volume pre-empted by the bubbles already present. The increase in the actual volume fraction of bubbles when new bubbles are added to the suspension is $d\phi/(1-\phi)$. Thus:

$$d\eta = \eta \left[\frac{1-\frac{12}{5}\left(\frac{\dot{\gamma}\eta R}{\sigma}\right)^2}{1+\left(\frac{6}{5}\frac{\dot{\gamma}\eta R}{\sigma}\right)^2} \right] \frac{d\phi}{1-\phi} \quad (12)$$

Upon integration with the limit $\eta \rightarrow \eta_c$ at $\phi \rightarrow 0$, Eq. 12 gives:

$$\eta_r \left[\frac{1-\frac{12}{5}\eta_r^2 N_{Ca}^2}{1-\frac{12}{5}N_{Ca}^2} \right]^{-4/5} = (1-\phi)^{-1} \quad (13)$$

This equation, referred to as 'model 2' in the remainder of the paper, reduces to the following equations:

$$N_{Ca} \rightarrow 0, \quad \eta_r = (1-\phi)^{-1} = 1 + \phi + \frac{\phi^2}{2} + \ldots \quad (14)$$

$$N_{Ca} \rightarrow \infty, \quad \eta_r = (1-\phi)^{5/3} = 1 - \frac{5}{3}\phi + \frac{5}{9}\phi^2 + \ldots \quad (15)$$

Thus, model 2 is consistent with the results for a dilute system.

One limitation of models 1 and 2 is that they fail to account for the so-called 'crowding effect' caused by packing difficulty of bubbles at high ϕ [50–52]. Due to immobilization of some of the continuous-phase fluid in the voids between the existing bubbles, the free volume of the continuous-phase fluid available when new bubbles are added is significantly less than $(1-\phi)$. Accord-

ingly, Mooney [50], in the derivation of his well-known equation for the viscosity of concentrated suspensions of rigid particles, contended that the incremental increase in the volume fraction of the dispersed phase when infinitesimal amounts of new particles are added to an existing suspension of dispersed phase volume fraction ϕ, is $d[\phi/(1-\phi/\phi_m)]$ rather than $d\phi/(1-\phi)$ as used in the derivation of model 2 (Eq. 13). Note that ϕ_m is the maximum packing volume fraction of undeformed spherical bubbles; for random close packing of monosized spherical bubbles, ϕ_m is 0.637. Thus, Eq. 7 becomes:

$$d\eta = \eta \left[\frac{1-\frac{12}{5}\left(\frac{\dot{\gamma}\eta R}{\sigma}\right)^2}{1+\left(\frac{6}{5}\frac{\dot{\gamma}\eta R}{\sigma}\right)^2}\right] d\left(\frac{\phi}{1-\frac{\phi}{\phi_m}}\right) \tag{16}$$

Upon integration, Eq. 16 gives:

$$\eta_r \left[\frac{1-\frac{12}{5}\eta_r^2 N_{Ca}^2}{1-\frac{12}{5}N_{Ca}^2}\right]^{-4/5} = \exp\left[\frac{\phi}{1-\frac{\phi}{\phi_m}}\right] \tag{17}$$

This equation, referred to as 'model 3' in the remainder of the paper, reduces to the following equations:

$$N_{Ca} \to 0, \quad \eta_r = \exp\left(\frac{\phi}{1-\frac{\phi}{\phi_m}}\right) \tag{18}$$

$$N_{Ca} \to \infty, \quad \eta_r = \exp\left(\frac{-5\phi/3}{1-\frac{\phi}{\phi_m}}\right) \tag{19}$$

Krieger and Dougherty [52], in the derivation of their well-known equation for the viscosity of concentrated suspensions of rigid particles, argued that the incremental increase in the volume fraction of the dispersed phase when a small amount of new particles is added to an existing suspension of concentration ϕ, is $d\phi/(1-\phi/\phi_m)$ rather than $d[\phi/(1-\phi/\phi_m)]$ as thought by Mooney [50]. Hence, Eq. 7 becomes:

$$d\eta = \eta \left[\frac{1-\frac{12}{5}\left(\frac{\dot{\gamma}\eta R}{\sigma}\right)^2}{1+\left(\frac{6}{5}\frac{\dot{\gamma}\eta R}{\sigma}\right)^2}\right] \left(\frac{d\phi}{1-\frac{\phi}{\phi_m}}\right) \tag{20}$$

Upon integration with the limit $\eta \to \eta_c$ at $\phi = 0$, Eq. 20 gives:

$$\eta_r \left[\frac{1-\frac{12}{5}\eta_r^2 N_{Ca}^2}{1-\frac{12}{5}N_{Ca}^2}\right]^{-4/5} = \left[1-\frac{\phi}{\phi_m}\right]^{-\phi_m} \tag{21}$$

This equation, referred to as 'model 4' in the remainder of the paper, reduces to the following equations:

$$N_{Ca} \to 0 \quad \eta_r = \left(1-\frac{\phi}{\phi_m}\right)^{-\phi_m} \tag{22}$$

$$N_{Ca} \to \infty \quad \eta_r = \left(1-\frac{\phi}{\phi_m}\right)^{5\phi_m/3} \tag{23}$$

As ϕ_m, the maximum packing volume fraction of undeformed bubbles, is sensitive to the bubble size distribution, models 3 and 4 are capable of taking into account the effect of the bubble size distribution on the viscosity of suspensions. An increase in ϕ_m occurs when a monodisperse suspension is changed to a polydisperse suspension.

Fig. 2 shows the relative viscosities predicted from models 1–4. All models predict that the relative viscosity at any given value of bubble volume fraction ϕ decreases with the increase in the capillary number, N_{Ca}. At low capillary numbers ($N_{Ca} < 0.645$), the relative viscosity increases with the increase in bubble volume fraction. At high capillary numbers ($N_{Ca} > 0.645$), an opposite effect is observed, that is, the relative viscosity decreases with the increase in ϕ. At a capillary number of 0.645, the relative viscosity is independent of ϕ; the relative viscosity is 1 for all values of ϕ.

4. Comparison of new viscosity equations with literature data

Seven sets of literature data on relative viscosity of bubbly suspensions are considered to evaluate

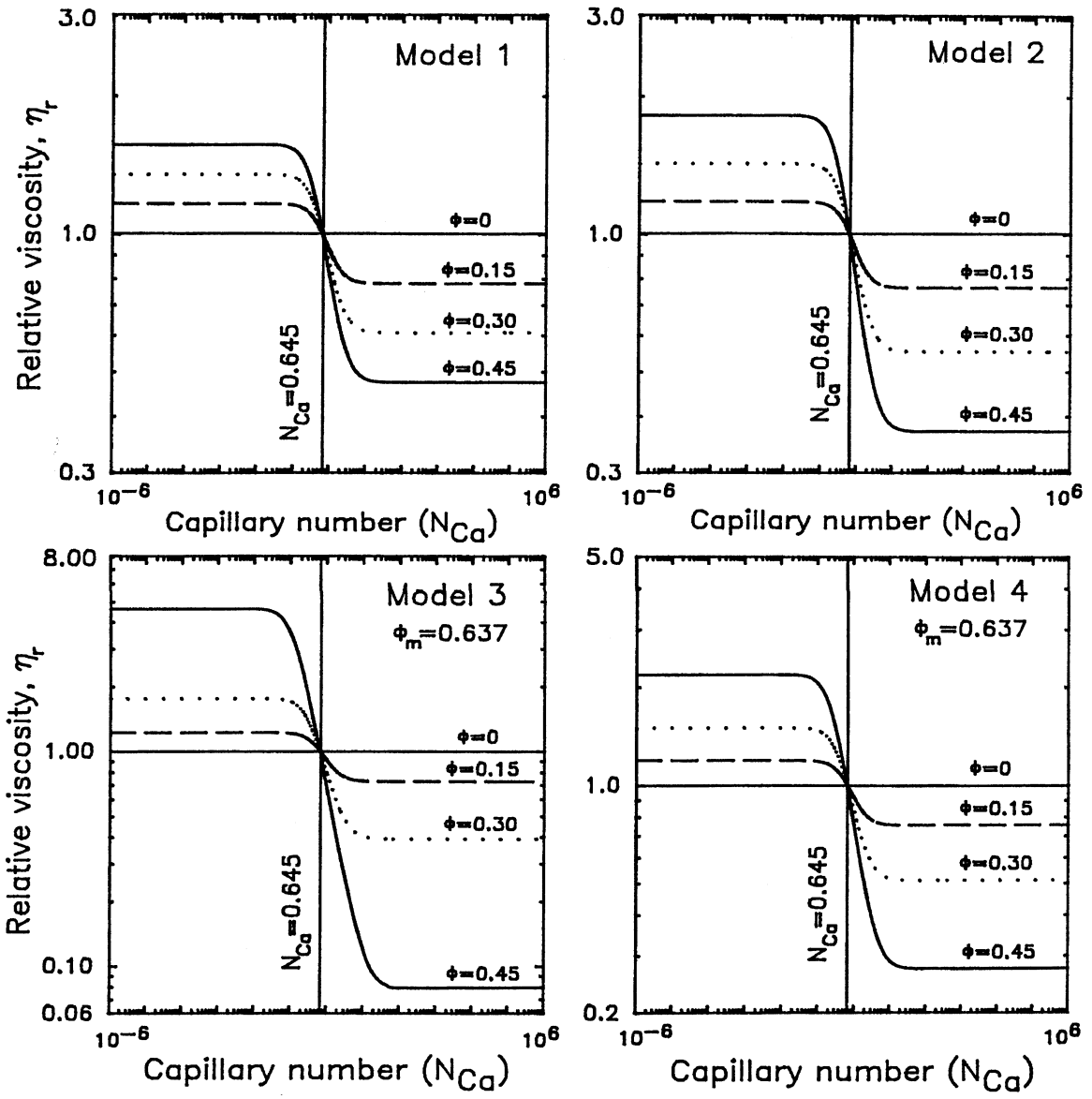

Fig. 2. Relative viscosity (η_r) as a function of capillary number (N_{Ca}) predicted by the proposed models. The predictions are shown for various values of bubble volume fraction (ϕ).

the models developed in this paper. The data are described only briefly here; further details about these data can be found in the original references. Lejeune et al. [1] measured the relative viscosities of bubble-bearing calcium aluminosilicate melts at different temperatures. The experiments were conducted in the high N_{Ca} regime. The bubble volume fractions were $\phi = 0$, 0.06, 0.13, 0.32, 0.41 and 0.47. At any given ϕ, the relative viscosity used in our analysis covers the temperature range of 1160–1220 K. Manga and Loewenberg [6] determined the relative viscosities of bubbly suspensions at high N_{Ca} ($N_{Ca} \rightarrow \infty$) using a numerical approach. Numerical calculations were performed using the boundary integral method. The bubble volume fraction was varied from 0 to 0.40. Rust

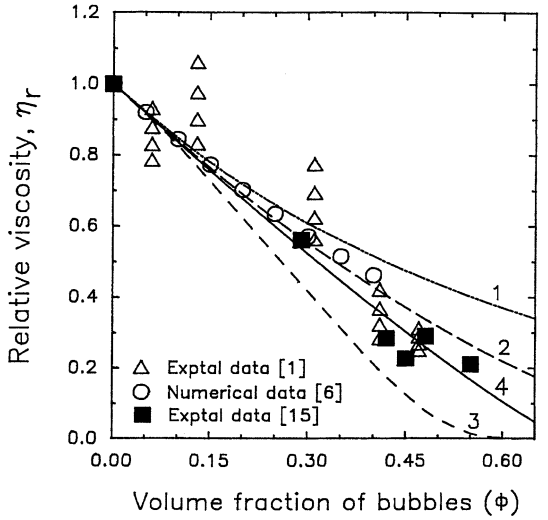

Fig. 3. Comparison between published data and predictions of various models at high N_{Ca}. ϕ_m is taken to be 0.70 for models 3 and 4. The numbers shown in the figure refer to model numbers.

and Manga [10] measured the relative viscosity of dilute bubbly suspensions with a rotating cylinder viscometer. Corn syrup of high viscosity (180 Pa s at 22°C) was used as the continuous phase and air bubbles as the dispersed phase. The relative viscosity measurements were limited to $N_{Ca} < 3$. Stein and Spera [15] measured the viscosities of rhyolite melt–bubble emulsions at temperatures in the range 925–1150°C. The bubble volume fraction was varied from 0.29 to 0.55. The experiments were conducted in the high N_{Ca} range of 30–925. Pal [53,54] studied the rheology of oil-in-water type emulsions consisting of low viscosity droplets suspended in a high viscosity matrix. Two sets of Pal's data are considered in our analysis; in one set [53], the ratio of dispersed phase viscosity to continuous phase viscosity was approximately 4.15×10^{-3} and in the other set [54], the ratio of dispersed phase viscosity to continuous phase viscosity was about 3.9×10^{-4}. As the viscosity ratio for these emulsions is very small, they can be regarded as bubbly suspensions; only the zero-shear relative viscosity data ($N_{Ca}\rightarrow0$) are considered in our analysis. Llewellin et al. [37] measured the linear viscoelastic properties of suspensions of nitrogen bubbles in a Newtonian liquid (golden syrup). The data were obtained using a parallel plate geometry in oscillatory mode. The volume fraction of bubbles was varied from 0 to 0.461. Their complex viscosity data at low oscillation frequency ($N_{Ca}\rightarrow0$) of imposed shear stress (amplitude well within the linear viscoelastic region) are considered in our analysis.

Fig. 3 shows a comparison between the published data and predictions of various models developed in the paper. The capillary number is large ($N_{Ca}\rightarrow\infty$) in this case. Model 1 (Eq. 9) describes the data reasonably well only at low to moderate values of ϕ ($\phi<0.30$); at higher values of ϕ, model 1 tends to overpredict the relative viscosity η_r, as expected. Model 2 (Eq. 13) is an improvement over model 1; it does a reasonable job in predicting the relative viscosity up to a ϕ value of 0.40. Note that there are no adjustable parameters in models 1 and 2. The predictions of models 3 (Eq. 17) and 4 (Eq. 21) are also shown in Fig. 3. These models contain ϕ_m, the maximum packing volume fraction of undeformed bubbles. Model 4 (Eq. 21) does a reasonable job over the full ϕ range covered by the published data, provided that a ϕ_m value of 0.7 is used. Model 3 (Eq. 17), however, underpredicts the relative viscosity for most of the ϕ range ($\phi>0.1$) when the same value of ϕ_m ($=0.70$) is used. The ϕ_m value of 0.70 is physically realistic and is close to the body-centered cubic packing of uniform spheres, i.e. $\phi_m=0.68$.

It is worthwhile to point out that some of the scatter in published data shown in Fig. 3 could be due to lack of steady state in some of these experiments [37]. Strictly speaking, the suspension should be subjected to shear for a duration larger than the relaxation time of bubbles β, defined as:

$$\beta=\frac{\eta_c R}{\sigma} \tag{24}$$

When the measurement time is larger than the bubble relaxation time β, the bubble deformation becomes constant. For some of the suspensions shown in Fig. 3, the bubble relaxation time was higher than the measurement time [37]. For example, the bubble relaxation time for porous glasses used by Lejeune et al. [1] is of the order of 50 min whereas their experiments ran for 'tens of minutes'.

Figs. 4 and 5 show the experimental data of

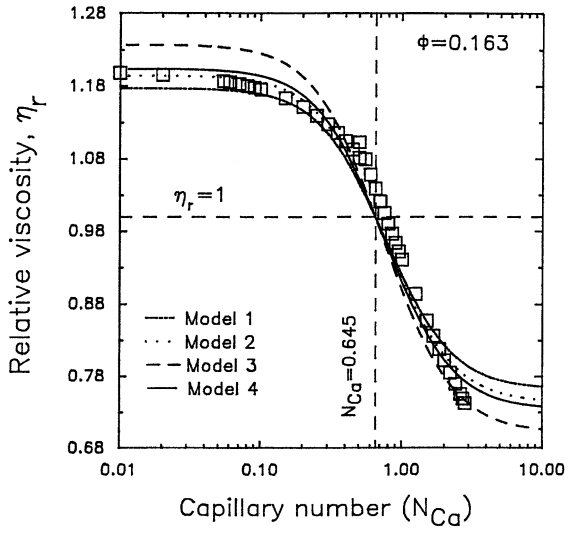

Fig. 4. Comparison between experimental data of Rust and Manga [10] and predictions of various models for $\phi = 0.163$. ϕ_m is taken to be 0.70 for models 3 and 4.

Rust and Manga [10] for suspensions with bubble volume fractions of 0.163 and 0.115, respectively. The data are plotted as relative viscosity versus capillary number. As the suspensions were polydisperse, an average bubble radius was used in the calculation of capillary number. The experimental data cover a broad range of N_{Ca}. The predictions of the models developed in the paper are also shown. For models 3 and 4, the ϕ_m value of 0.70 (the same as that used before in Fig. 3) was utilized. The trends exhibited by all four models are in good agreement with the experimental data. At low values of N_{Ca}, model 1 underpredicts η_r whereas model 3 overpredicts η_r. The predictions of models 2 and 4 are similar and are in good agreement with the experimental data over a wide range of N_{Ca}. It is interesting to note that the experimental measurements give η_r of approximately 1 at a N_{Ca} value of 0.645, as predicted by the models.

Fig. 6 shows a comparison between the experimental data of Pal [53,54] and predictions of various models. The capillary number is small ($N_{Ca} \to 0$) in this case. As can be seen, the experimental data can be described reasonably well with model 4 (Eq. 21) using a ϕ_m value of 0.54. The ϕ_m value of 0.54 is close to simple cubic packing of monodisperse spheres, i.e. $\phi_m = 0.52$. For the same ϕ_m value, model 3 (Eq. 17) overpredicts the relative viscosity, especially when $\phi > 0.20$.

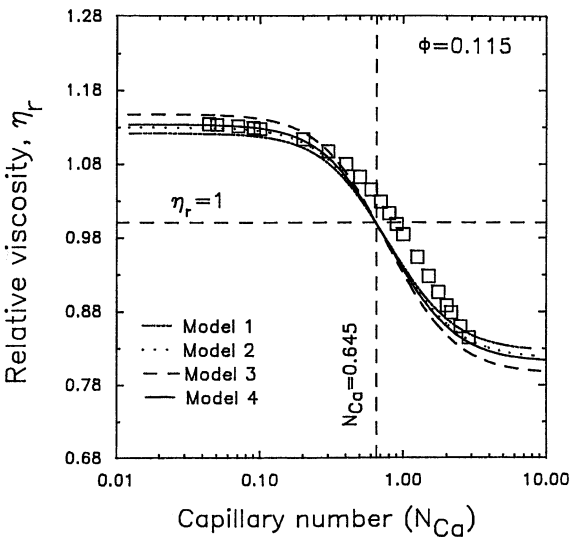

Fig. 5. Comparison between experimental data of Rust and Manga [10] and predictions of various models for $\phi = 0.115$. ϕ_m is taken to be 0.70 for models 3 and 4.

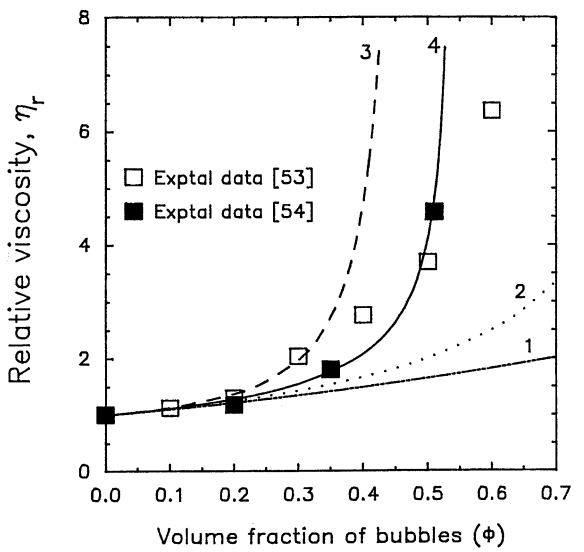

Fig. 6. Comparison between experimental data of Pal [53,54] and predictions of various models at low N_{Ca} ($N_{Ca} \to 0$). ϕ_m is taken to be 0.54 for models 3 and 4. The numbers shown in the figure refer to model numbers.

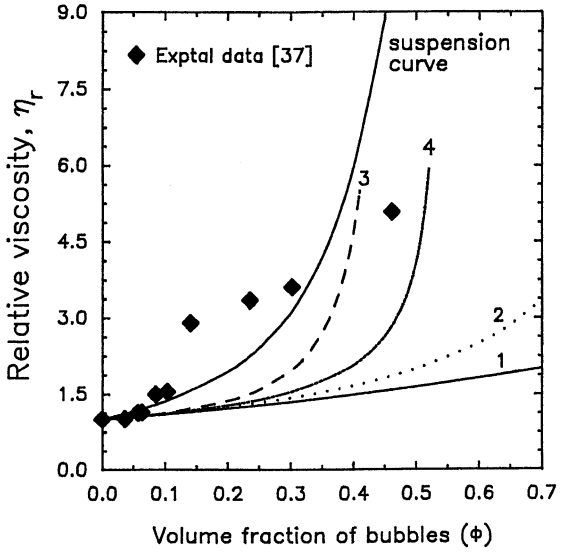

Fig. 7. Comparison between experimental data of Llewellin et al. [37] and predictions of various models at low N_{Ca} ($N_{Ca} \rightarrow 0$). ϕ_m is taken to be 0.54 for models 3 and 4. The numbers shown in the figure refer to model numbers. The solids-in-liquid suspension curve [55] is also shown for comparison purposes.

Models 1 (Eq. 9) and 2 (Eq. 13) underpredict η_r when $\phi > 0.20$.

Fig. 7 shows the experimental data of Llewellin et al. [37] at low oscillation frequency of imposed shear stress. The predictions of models 1–4 are also shown; the ϕ_m value for models 3 and 4 is taken to be 0.54 (the same as that used for Pal's data, Fig. 6). The solids-in-liquid suspension curve [55], in terms of relative viscosity versus volume fraction of solids, is shown as well for comparison purposes. Clearly, the proposed models (models 1–4) do not describe Llewellin et al.'s data satisfactorily. However, it should be noted that the relative viscosities of bubbly suspensions studied by Llewellin et al. are even higher than those of solids-in-liquid suspensions in the ϕ range of 0.1–0.3. This is physically unrealistic. Several factors could be responsible for the anomalous behavior exhibited by Llewellin et al.'s bubbly suspensions; they are summarized as follows: (1) They utilized the parallel plate geometry which does not impart uniform shear rate to the sample. Extraction of the rheological parameters from the raw data obtained from this technique is not trivial as the strain varies with the radius. The authors do not address this issue in their paper; (2) The measurements were affected by bubble-rise/creaming effect, as the authors freely admit in their paper. The bubble-rise effect would render the suspension sample non-homogeneous; (3) There were uncertainties in the value of the continuous-phase (syrup) viscosity, used in their calculation of relative viscosity. The continuous-phase viscosity changed during the aeration process; (4) Slip effects [56] have not been considered in their work. Slip is well known to occur during the flow of suspensions between smooth solid boundaries with narrow gaps. The only way to check if slip effects are absent is to obtain data from different gap widths. In the absence of slip effects, the data are independent of the gap width; and (5) Their complex viscosity data do not exhibit a plateau at low frequencies, as assumed in their curve fitting exercise. At high values of ϕ, their measured complex viscosity continues to increase with the decrease in frequency. Thus, their low frequency limiting values of relative viscosity, shown in Fig. 7, are questionable.

In summary, model 4 (Eq. 21) appears to be somewhat superior to other models (models 1–3) developed in the paper when comparisons are made with the limited amount of experimental and numerical data available in the published literature. Furthermore, model 4 is quite capable of predicting the effect of bubble size distribution on the viscosity of bubble-bearing suspensions, as discussed in the following section.

5. Effect of bubble size distribution on the viscosity of suspensions

The effect of bubble size distribution on the relative viscosity of bubbly suspensions can be predicted from model 4 (Eq. 21). Model 4 contains ϕ_m, the maximum packing volume fraction of bubbles, which is known to be sensitive to bubble/particle size distribution; ϕ_m for suspensions of uniform bubbles is expected to be significantly smaller as compared with the ϕ_m value for polydisperse suspensions. Note that ϕ_m in model 4

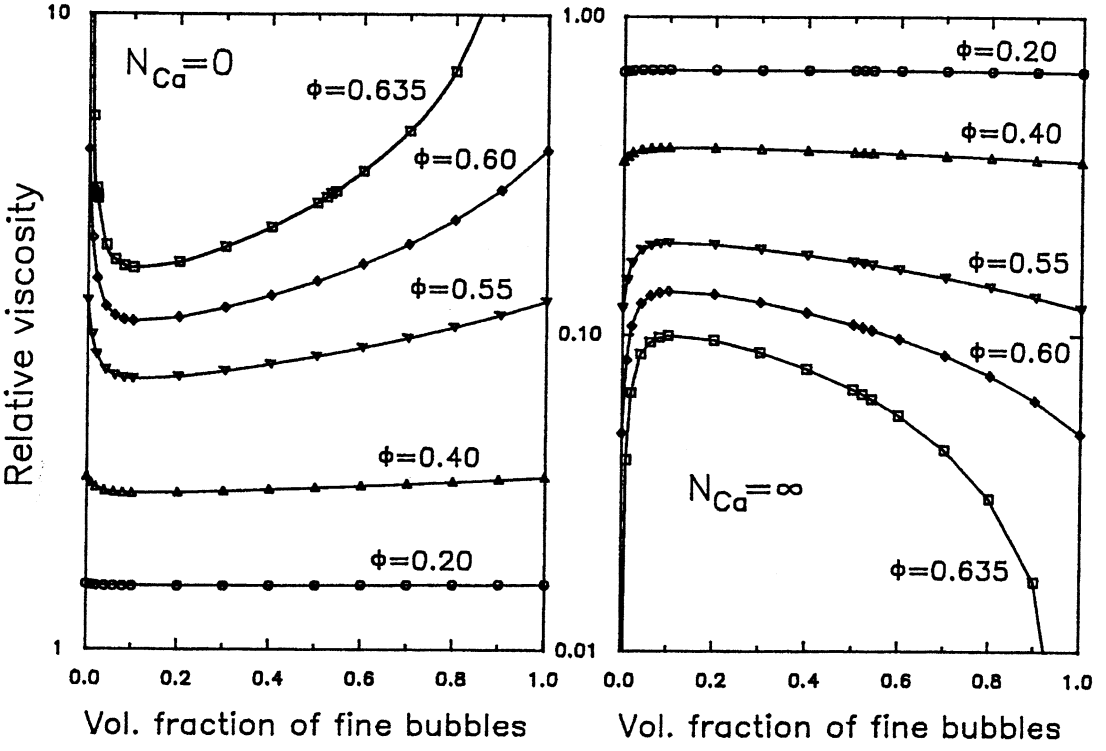

Fig. 8. The effect of bubble size distribution on the relative viscosity of bimodal suspensions, as predicted from model 4. The bubble size ratio between large and small bubbles is 5:1.

(and model 3) refers to the initial undeformed state of the suspension, just like R refers to the radius of undeformed bubbles in the initial undeformed state of the suspension. The effect of bubble deformation on the viscosity of suspension is accounted for by the capillary number alone. Thus, ϕ_m depends only on the size distribution of initial undeformed bubbles.

It is well known that polydispersity tends to increase ϕ_m. Ouchiyama and Tanaka [57–59] have published a series of articles aimed at estimating the porosity $(1-\phi_m)$ of random packings of spherical particles having various sizes. According to Ouchiyama and Tanaka's theory [57–59], the maximum packing volume fraction is given by:

$$\phi_m = \frac{\sum D_i^3 f_i}{\sum (D_i \sim \overline{D})^3 f_i + \frac{1}{\alpha}\sum[(D_i+\overline{D})^3-(D_i\sim\overline{D})^3]f_i} \quad (25)$$

where:

$$\alpha = 1+\frac{4}{13}(8\phi_m^o-1)\overline{D}$$

$$\frac{\sum (D_i+\overline{D})^2\left[1-\frac{(3/8)\overline{D}}{(D_i+\overline{D})}\right]f_i}{\sum[D_i^3-(D_i\sim\overline{D})^3]f_i} \quad (26)$$

$$\overline{D} = \sum D_i f_i \quad (27)$$

Here ϕ_m^o is the maximum packing concentration of a monodisperse suspension, f_i is the number fraction of droplets of diameter D_i, $\overline{D}$ is the number-average diameter of the suspension, and the abbreviation $(D_i \sim \overline{D})$ is defined as:

$$(D_i\sim\overline{D}) = 0 \text{ for } D_i \le \overline{D} \quad (28)$$

$$= D_i - \overline{D} \text{ for } D_i > \overline{D} \quad (29)$$

To calculate ϕ_m for polydisperse suspensions using the Ouchiyama and Tanaka theory (Eqs. 25–29), the value of the maximum packing concen-

tration of the monodisperse suspension (ϕ_m^o) is required.

We utilized Eqs. 25–29 to predict ϕ_m values for bimodal suspensions of bubbles, that is, mixtures of two bubble sizes: large and small. The bubble size ratio was taken to be 5:1. The ϕ_m value for monodisperse suspension (ϕ_m^o) was taken to be 0.637, corresponding to random close packing of spheres.

With the increase in the proportion of fine bubbles in a bimodal suspension, the value of ϕ_m increased initially, reached a maximum value of approximately 0.76 at a fine bubble proportion of about 10%, and then decreased. The ϕ_m values, calculated for different proportions of fine bubbles using Eqs. 25–29, were used to calculate the relative viscosities from model 4.

Fig. 8 shows the effect of bubble size distribution on the relative viscosity of bimodal suspensions at two different values of capillary number, N_{Ca}: $N_{Ca} = 0$ and $N_{Ca} = \infty$. The relative viscosities predicted from model 4 are plotted as a function of the volume fraction of fine bubbles present in a bimodal suspension, with total volume fraction as a parameter. At low N_{Ca}, Fig. 8 reveals the following information: (a) a large reduction in relative viscosity occurs when a concentrated ($\phi \geq 0.55$) monodisperse suspension is changed to a bimodal suspension; this effect is negligible when $\phi \leq 0.40$; (b) at high values of ϕ, the plots of relative viscosity vs. volume fraction of fine bubbles exhibit a minimum at a fine bubble volume fraction of about 0.1 (where a maximum in ϕ_m occurs). At high N_{Ca}, Fig. 8 shows a very different behavior: (a) the relative viscosity now exhibits an opposite effect, that is, it increases when a concentrated ($\phi \geq 0.55$) monodisperse suspension is changed to a bimodal suspension; this effect is negligible when $\phi \leq 0.40$; (b) the plots of relative viscosity vs. volume fraction of fine bubbles, at high values of ϕ, exhibit a maximum at a fine bubble volume fraction of about 0.1.

6. Concluding remarks

Starting from the relative viscosity equation of dilute suspension of bubbles, four new equations are developed for concentrated bubbly suspensions using a differential scheme. According to the proposed equations, the relative viscosity (η_r) versus capillary number (N_{Ca}) plots exhibit three distinct regions: constant η_r region at low values of N_{Ca}, decreasing η_r region at intermediate values of N_{Ca}, and, finally, constant η_r region at high values of N_{Ca}. The relative viscosity is greater than unity at low N_{Ca} ($N_{Ca} < 0.645$) and is less than unity at high N_{Ca} ($N_{Ca} > 0.645$). With the increase in the bubble volume fraction (ϕ), η_r increases at low N_{Ca} and decreases at high N_{Ca}. At $N_{Ca} = 0.645$, η_r is unity independent of ϕ. Out of the four models developed in the paper, two models (models 1 and 2) predict η_r to be a function of only two variables: N_{Ca} and ϕ; these models do not contain any adjustable parameters. The remaining two models (models 3 and 4) contain an additional parameter, that is, the maximum packing volume fraction of bubbles (ϕ_m).

Model 4 (Eq. 21) appears to be somewhat superior to other models (models 1–3) developed in the paper when comparisons are made with the limited amount of experimental and numerical data available in the literature. Furthermore, model 4 is quite capable of predicting the effect of bubble size distribution on the viscosity of bubble-bearing magmas. At low N_{Ca}, a large reduction in relative viscosity occurs when a concentrated ($\phi \geq 0.55$) monodisperse suspension is changed to a bimodal suspension. At high N_{Ca}, an opposite effect is observed, that is, a large increase in relative viscosity occurs when a concentrated monodisperse suspension is changed to a bimodal suspension.

The viscosity models for bubble-bearing suspensions developed in this study are useful in modeling of the volcanic processes.

Acknowledgements

Financial support from the Natural Sciences and Engineering Research Council of Canada is appreciated. *[SK]*

Appendix A. Derivation of Eq. 4 from Eq. 3

In steady viscometric flow, the velocity is given by $\hat{V}=(\dot{\gamma}x_2,0,0)$, where $\dot{\gamma}$ is the shear rate. In this case,

$$\nabla\hat{V}=\begin{pmatrix}0&0&0\\1&0&0\\0&0&0\end{pmatrix}\dot{\gamma},\quad(\nabla\hat{V})^{\mathrm{T}}=\begin{pmatrix}0&1&0\\0&0&0\\0&0&0\end{pmatrix}\dot{\gamma}\tag{A1}$$

$$\overline{d}\overset{\mathrm{def}}{=}\frac{1}{2}[(\nabla\hat{V})+(\nabla\hat{V})^{\mathrm{T}}]=\frac{\dot{\gamma}}{2}\begin{pmatrix}0&1&0\\1&0&0\\0&0&0\end{pmatrix}\tag{A2}$$

$$\overline{\omega}\overset{\mathrm{def}}{=}\frac{1}{2}[(\nabla\hat{V})-(\nabla\hat{V})^{\mathrm{T}}]=\frac{\dot{\gamma}}{2}\begin{pmatrix}0&-1&0\\1&0&0\\0&0&0\end{pmatrix}\tag{A3}$$

Here $\overline{\mathrm{d}}$ is the rate of deformation tensor and $\overline{\omega}$ is the vorticity tensor. The Jaumann derivatives in Eq. 3 for viscometric flows are:

$$\frac{\mathrm{D}\overline{d}}{\mathrm{D}t}\overset{\mathrm{def}}{=}\frac{\partial\overline{d}}{\partial t}+\hat{V}\cdot\nabla\overline{d}+\overline{\omega}\cdot\overline{d}-\overline{d}\cdot\overline{\omega}=\frac{\dot{\gamma}^2}{2}\begin{pmatrix}-1&0&0\\0&1&0\\0&0&0\end{pmatrix}\tag{A4}$$

$$\frac{\mathrm{D}\overline{\tau}}{\mathrm{D}t}\overset{\mathrm{def}}{=}\frac{\partial\overline{\tau}}{\partial t}+\hat{V}\cdot\nabla\overline{\tau}+\overline{\omega}\cdot\overline{\tau}-\overline{\tau}\cdot\overline{\omega}=\frac{\dot{\gamma}}{2}\begin{pmatrix}-2\tau_{12}&\tau_{11}-\tau_{22}&0\\\tau_{11}-\tau_{22}&2\tau_{12}&0\\0&0&0\end{pmatrix}\tag{A5}$$

The term $[\overline{d}\cdot\overline{d}+\overline{d}^{\mathrm{T}}\cdot\overline{d}^{\mathrm{T}}-(2/3)\mathrm{tr}(\overline{d}\cdot\overline{d})\overline{\delta}]$ in Eq. 3 reduces to:

$$\overline{d}\cdot\overline{d}+\overline{d}^{\mathrm{T}}\cdot\overline{d}^{\mathrm{T}}-\frac{2}{3}\mathrm{tr}(\overline{d}\cdot\overline{d})\overline{\delta}=\frac{\dot{\gamma}^2}{6}\begin{pmatrix}1&0&0\\0&1&0\\0&0&-2\end{pmatrix}\tag{A6}$$

Thus, Eq. 3 can be written as:

$$\begin{pmatrix}\tau_{11}&\tau_{12}&0\\\tau_{21}&\tau_{22}&0\\0&0&\tau_{33}\end{pmatrix}+\frac{\Lambda\dot{\gamma}}{2}\begin{pmatrix}-2\tau_{12}&\tau_{11}-\tau_{22}&0\\\tau_{11}-\tau_{22}&2\tau_{12}&0\\0&0&0\end{pmatrix}$$
$$=2\eta_{\mathrm{c}}(1+\phi)\left[\frac{\dot{\gamma}}{2}\begin{pmatrix}0&1&0\\1&0&0\\0&0&0\end{pmatrix}+\frac{\Lambda\dot{\gamma}^2}{2}\begin{pmatrix}-1&0&0\\0&1&0\\0&0&0\end{pmatrix}\right]+\left(\frac{\eta_{\mathrm{c}}^2R}{\sigma}\phi\right)\left[-\frac{16}{5}\dot{\gamma}^2\begin{pmatrix}-1&0&0\\0&1&0\\0&0&0\end{pmatrix}+\frac{4}{35}\dot{\gamma}^2\begin{pmatrix}1&0&0\\0&1&0\\0&0&-2\end{pmatrix}\right]\tag{A7}$$

Comparing terms yields the following set of equations:

$$\tau_{11}-\Lambda\dot{\gamma}\tau_{12}=\eta_{\mathrm{c}}\dot{\gamma}^2\Lambda\left(-1+\frac{37}{21}\phi\right)\tag{A8}$$

$$\tau_{12}+\frac{\Lambda\dot{\gamma}}{2}(\tau_{11}-\tau_{22})=\eta_{\mathrm{c}}\dot{\gamma}(1+\phi)\tag{A9}$$

$$\tau_{22}+\Lambda\dot{\gamma}\tau_{12}=\eta_{\mathrm{c}}\dot{\gamma}^2\Lambda\left[1-\frac{11}{7}\phi\right]\tag{A10}$$

$$\tau_{33}=\frac{-4\eta_{\mathrm{c}}\dot{\gamma}^2\Lambda\phi}{21}\tag{A11}$$

Eqs. A8–A10 yield the following expression for shear stress:

$$\tau_{12}=\frac{\eta_{\mathrm{c}}\dot{\gamma}}{1+\Lambda^2\dot{\gamma}^2}(1+\phi)+\frac{\eta_{\mathrm{c}}\Lambda^2\dot{\gamma}^3}{1+\Lambda^2\dot{\gamma}^2}\left(1-\frac{5}{3}\phi\right)=\eta_{\mathrm{c}}\dot{\gamma}\left[1+\phi\left(\frac{1-\frac{5}{3}\Lambda^2\dot{\gamma}^2}{1+\Lambda^2\dot{\gamma}^2}\right)\right]\tag{A12}$$

Using the definitions of viscosity (ratio of shear stress to shear rate), relative viscosity (ratio of suspension viscosity η to continuous-phase viscosity η_{c}), and Λ ($=6\eta_{\mathrm{c}}R/5\sigma$), Eq. A12 yields:

$$\eta_{\mathrm{r}}=\frac{\eta}{\eta_{\mathrm{c}}}=1+\phi\left[\frac{1-\left(\frac{12}{5}N_{\mathrm{Ca}}^2\right)}{1+\left(\frac{6}{5}N_{\mathrm{Ca}}\right)^2}\right]\tag{A13}$$

where N_{Ca} is the capillary number defined in Eq. 5. Eq. A13 is the same as Eq. 4.

References

[1] A.M. Lejeune, Y. Bottinga, T.W. Trull, P. Richet, Rheology of bubble-bearing magmas, Earth Planet. Sci. Lett. 166 (1999) 71–84.

[2] F.J. Spera, D.J. Stein, Comment on 'Rheology of bubble-bearing magmas' by Lejeune et al., Earth Planet. Sci. Lett. 175 (2000) 327–331.

[3] A.M. Lejeune, Y. Bottinga, T.W. Trull, P. Richet, Rheology of bubble-bearing magmas: reply to a critical comment by Spera and Stein, Earth Planet. Sci. Lett. 175 (2000) 333–334.

[4] D.J. Stein, F.J. Spera, Rheology and microstructure of magmatic emulsions: theory and experiments, J. Volcanol. Geotherm. Res. 49 (1992) 157–174.

[5] M. Manga, J. Castro, K.V. Cashman, M. Loewenberg, Rheology of bubble-bearing magmas, J. Volcanol. Geotherm. Res. 87 (1998) 15–28.

[6] M. Manga, M. Loewenberg, Viscosity of magmas containing highly deformable bubbles, J. Volcanol. Geotherm. Res. 105 (2001) 19–24.

[7] H. Massol, C. Jaupart, The generation of gas overpressure in volcanic eruptions, Earth Planet. Sci. Lett. 166 (1999) 57–70.

[8] R.S.J. Sparks, Causes and consequences of pressurisation in lava dome eruptions, Earth Planet. Sci. Lett. 150 (1997) 177–189.

[9] C. Jaupart, C.J. Allegre, Gas content, eruption rate and instabilities of eruption regime in silicic volcanoes, Earth Planet. Sci. Lett. 102 (1991) 413–429.

[10] A.C. Rust, M. Manga, Effects of bubble deformation on the viscosity of dilute suspensions, J. Non-Newtonian Fluid Mech. 104 (2002) 53–63.

[11] H. Pinkerton, G. Norton, Rheological properties of basaltic lavas at sub-liquidus temperatures: laboratory and field measurements on lavas from Mount Etna, J. Volcanol. Geotherm. Res. 68 (1995) 307–323.

[12] H. Pinkerton, R.J. Stevenson, Methods of determining the rheological properties of magmas at sub-liquidus temperatures, J. Volcanol. Geotherm. Res. 53 (1992) 47–66.

[13] F. Dobran, Non equilibrium flow in volcanic conduits and application to the eruptions of Mt. St. Helens on May 18, 1980, and Vesuvius in AD 79, J. Volcanol. Geotherm. Res. 49 (1992) 285–311.

[14] N.S. Bogdassarov, D.B. Dingwell, A rheological investigation of vesicular rhyolite, J. Volcanol. Geotherm. Res. 50 (1992) 307–322.

[15] D.J. Stein, F.J. Spera, Shear viscosity of rhyolite - vapor emulsions at magmatic temperatures by concentric cylinder rheometry, J. Volcanol. Geotherm. Res. 113 (2002) 243–258.

[16] Y. Liu, Y. Zhang, Bubble growth in rhyolitic melt, Earth Planet. Sci. Lett. 181 (2000) 251–264.

[17] S. Hurwitz, O. Navon, Bubble nucleation in rhyolitic melts: experiments at high pressure, temperature, and water content, Earth Planet. Sci. Lett. 122 (1994) 267–280.

[18] O. Navon, A. Chekhmir, V. Lyakhovsky, Bubble growth in highly viscous melts: theory, experiments, and autoexplosivity of dome lavas, Earth Planet. Sci. Lett. 160 (1998) 763–776.

[19] J.E. Gardner, M. Hilton, M.R. Carroll, Experimental constraints on degassing of magma: isothermal bubble growth during continuous decompression from high pressure, Earth Planet. Sci. Lett. 168 (1999) 201–218.

[20] J.F. Larsen, J.E. Gardner, Experimental constraints on bubble interactions in rhyolite melts: implications for vesicle size distribution, Earth Planet. Sci. Lett. 180 (2000) 201–214.

[21] R.J. Stevenson, N.S. Bagdassarov, C. Romano, Vesiculation processes in a water-rich calc-alkaline obsidian, Earth Planet. Sci. Lett. 146 (1997) 555–571.

[22] C. Martel, H. Bureau, In situ high-pressure and high-temperature bubble growth in silicic melts, Earth Planet. Sci. Lett. 191 (2001) 115–127.

[23] A.C. Rust, M. Manga, Bubble shapes and orientations in low Re simple shear flow, J. Colloid Interface Sci. 249 (2002) 476–480.

[24] N.G. Lensky, V. Lyakhovsky, O. Mavon, Radial variations of melt viscosity around growing bubbles and gas overpressure in vesiculating magmas, Earth Planet. Sci. Lett. 186 (2001) 1–6.

[25] J.D. Blower, H.M. Mader, S.D.R. Wilson, Coupling of viscous and diffusive controls on bubble growth during explosive volcanic eruptions, Earth Planet. Sci. Lett. 193 (2001) 47–56.

[26] H. Gaonac'h, S. Lovejoy, J. Stix, D. Scherzter, A scaling growth model for bubbles in basaltic lava flows, Earth Planet. Sci. Lett. 139 (1996) 395–409.

[27] S. Vergniolle, Bubble size distribution in magma and dynamics of basaltic eruptions, Earth Planet. Sci. Lett. 140 (1996) 269–279.

[28] R.S.J. Sparks, The dynamics of bubble formation and growth in magmas: A review and analysis, J. Volcanol. Geotherm. Res. 105 (2001) 19–24.

[29] A. Toramaru, Vesiculation process and bubble size distributions in ascending magmas with constant velocities, J. Geophys. Res. 94 (1989) 17523–17542.

[30] S.S.S. Cardoso, A.W. Woods, On convection in a volatile-saturated magma, Earth Planet. Sci. Lett. 168 (1999) 301–310.

[31] C. Martel, D.B. Dingwell, O. Spieler, M. Pichavant, M. Wilke, Fragmentation of foamed silicic melts: an experimental study, Earth Planet. Sci. Lett. 178 (2000) 47–58.

[32] H. Brenner, Suspension rheology, Prog. Heat Mass Transf. 5 (1972) 89–129.

[33] R. Pal, Viscosity-concentration equation for emulsions of nearly spherical droplets, J. Colloid Interface Sci. 231 (2000) 168–175.

[34] R. Pal, Evaluation of theoretical viscosity models for concentrated emulsions at low capillary numbers, Chem. Eng. J. 81 (2001) 15–21.

[35] R. Pal, Novel viscosity equations for emulsions of two immiscible liquids, J. Rheol. 45 (2001) 509–520.

[36] R. Pal, Single-parameter and two-parameter rheological

equations of state for nondilute emulsions, Ind. Eng. Chem. Res. 40 (2001) 5666–5674.
[37] E.W. Llewellin, H.M. Mader, S.D.R. Wilson, The rheology of a bubbly liquid, Proc. R. Soc. Lond. A 458 (2002) 987–1016.
[38] R. Pal, Oscillatory, creep and steady flow behaviour of xanthan-thickened oil-in-water emulsions, AIChE J. 41 (1995) 783–794.
[39] R. Pal, Effect of droplet size on the rheology of emulsions, AIChE J. 42 (1996) 3181–3190.
[40] R. Pal, Rheological behaviour of surfactant-flocculated water-in-oil emulsions, Colloids Surf. A 71 (1993) 173–185.
[41] G.I. Taylor, The viscosity of a fluid containing small drops of another liquid, Proc. R. Soc. Lond. A 138 (1932) 41–48.
[42] R. Pal, Anomalous effects in the flow behaviour of oil-in-water emulsions, Chem. Eng. J. 63 (1996) 195–199.
[43] N.A. Frankel, A. Acrivos, The constitutive equation for a dilute emulsion, J. Fluid Mech. 44 (1970) 65–78.
[44] H.C. Brinkman, The viscosity of concentrated suspensions and solutions, J. Chem. Phys. 20 (1952) 571.
[45] R. Roscoe, The viscosity of suspensions of rigid spheres, Br. J. Appl. Phys. 3 (1952) 267–269.
[46] A. Einstein, Eine neue Bestimmung der Molekuldimension, Ann. Phys. 19 (1906) 289–306.
[47] A. Einstein, Berichtigung zu meiner Arbeit: Eine neue Bestimmung der Molekuldimension, Ann. Phys. 34 (1911) 591–592.
[48] J.K. Mackenzie, Elastic constants of a solid containing spherical holes, Proc. Phys. Soc. Lond. B 63 (1950) 2–11.
[49] H. Chen, A. Acrivos, The effective moduli of composite materials containing spherical inclusions at non-dilute concentrations, Int. J. Solids Struct. 14 (1978) 349–364.
[50] M. Mooney, The viscosity of a concentrated suspension of spherical particles, J. Colloid Sci. 6 (1951) 162–170.
[51] R.D. Sudduth, A generalized model to predict the viscosity of solutions with suspended particles, J. Appl. Polym. Sci. 48 (1993) 25–36.
[52] I.M. Krieger, T.J. Dougherty, A mechanism for non-Newtonian flow in suspensions of rigid particles, Trans. Soc. Rheol. 3 (1959) 137–152.
[53] R. Pal, Rheological properties of emulsions of oil in aqueous non-Newtonian polymeric media, Chem. Eng. Commun. 111 (1992) 45–60.
[54] R. Pal, Viscoelastic properties of polymer-thickened oil-in-water emulsions, Chem. Eng. Sci. 51 (1996) 3299–3305.
[55] D.G. Thomas, Transport characteristics of suspensions: VIII. A note on the viscosity of Newtonian suspension of uniform spherical particles, J. Colloid Sci. 20 (1965) 267–277.
[56] H.A. Barnes, A review of the slip (wall depletion) of polymer solutions, emulsions and particle suspensions in viscometers: its causes, character, and cure, J. Non-Newtonian Fluid Mech. 56 (1995) 221–251.
[57] N. Ouchiyama, T. Tanaka, Estimation of the average number of contacts between randomly mixed solid particles, Ind. Eng. Chem. Fundam. 19 (1980) 338–340.
[58] N. Ouchiyama, T. Tanaka, Porosity of a mass of solid particles having a range of sizes, Ind. Eng. Chem. Fundam. 20 (1981) 66–71.
[59] N. Ouchiyama, T. Tanaka, Porosity estimation for random packings of spherical particles, Ind. Eng. Chem. Fundam. 23 (1984) 490–493.